Soft Matter

Bobbing chemical garden tubes: oscillatory self-motion from buoyancy and catalytic gas production

Journal:	*Soft Matter*
Manuscript ID	SM-ART-12-2022-001681.R1
Article Type:	Paper
Date Submitted by the Author:	07-Feb-2023
Complete List of Authors:	Wang, Qingpu; Florida State University, Department of Chemistry and Biochemistry Steinbock, Oliver; Florida State University, Department of Chemistry and Biochemistry

ARTICLE

Bobbing chemical garden tubes: oscillatory self-motion from buoyancy and catalytic gas production†

Qingpu Wang[‡a] and Oliver Steinbock*[a]

Received 00th January 20xx,
Accepted 00th January 20xx

DOI: 10.1039/x0xx00000x

Chemical reactions can induce self-propulsion by the production and ejection of gas bubbles from micro-rocket like cylindrical units. We describe related micro-submarines that change their depth in response to catalytic gas production. The structures consist of silica-supported CuO and are produced by utilizing the self-assembly rules of chemical gardens. In H_2O_2 solution, the tube cavity produces O_2(g) and the resulting buoyancy lifts the tube to the air-solution interface, where it releases oxygen and sinks back down to the bottom of the container. In 5-cm deep solutions, the resulting bobbing cycles have a period of 20-30 s and repeat for several hours. The ascent is characterized by a vertical orientation of the tube and a constant acceleration. During the descent, the tubes are oriented horizontally and sink at a nearly constant speed. These striking features are quantitatively captured by an analysis of the involved mechanical forces and chemical kinetics. The results show that ascending tubes increase their oxygen-production rate by the motion-induced injection of fresh solution into the tube cavity.

Introduction

The study of chemical oscillations has led to significant advances in our understanding of complex dynamics in far-from-equilibrium systems.[1] First observations of these oscillations were made for electrochemical reactions[2], but the existence of liquid phase oscillators remained controversial as the behavior was incorrectly perceived to be a violation of the second law of thermodynamics.[3] In the 1970s, pioneering theoretical work by Ilya Prigogine and others as well as careful experimental studies radically changed this situation and initiated a phase of systematic research on chemical oscillators.[4,5] Over the following decades, these advances revolutionized the understanding of biological rhythms in systems ranging from circadian clocks to beating heart cells[6] and clarified—often unwanted—oscillations in engineering systems such as fuel cells and catalytic converters[7,8].

An intriguing extension of nonlinear oscillations is the—integral or passively coupled—generation of motion.[9] In physics, a classic example is the salt-water (or density) oscillator which generates periodic fluid exchange across a small orifice connecting an upper compartment filled with heavy salt solution and a lower volume of water.[10] Chemical examples include oscillators in which the response of a gel causes autonomous shape changes and, in some cases, triggers active motion.[11,12]

Here, we report an example of density-driven oscillations based on catalytic precipitate tubes that belong to the large class of chemical gardens. First studied by alchemists in the 17th century, chemical gardens have become a standard demonstration experiment in classrooms across the world.[13] In the classical version of the experiment, small metal salt grains are submerged in sodium silicate solution (waterglass).[14,15] In response, the dissolving grains quickly surround themselves with a semi-permeable inorganic membrane which compartmentalizes the system. Subsequently, osmotic pressure drives an influx of water and the membrane bursts ejecting a jet of buoyant salt solution.[16] Tube growth occurs along the diffuse and reactive interface of this rising jet and self-extends in the upward direction.[17] These enigmatic processes typically occur within a few minutes and at length scales of micro- to centimeters.

Earlier studies by our group established controlled versions of the chemical garden experiment, in which salt solutions are steadily injected into waterglass or solutions of other precipitation partners.[18,19] These studies also showed that under certain conditions, the tube radius is determined by the resulting fluid flow.[20] Moreover, the tube walls were found to have a thickness of about 5-10 µm with a thin outer layer of amorphous silica and an inner layer of metal hydroxide or oxide.[21] We also note that, while fragile, the thin walled tubes can withstand postsynthetic transformations induced by heat or ion-replacement reactions.[22] For example, Roszol et al. reported the shape-preserving transformation of silica-Cu(OH)$_2$ tubes to silica-CuO, silica-Cu_2O, and even silica-Cu(0).[23]

[a] Department of Chemistry and Biochemistry, Florida State University, Tallahassee, FL 32306-4390, USA

[‡] Present address: Energy and Environment Directorate, Pacific Northwest National Laboratory, Seattle, WA 98109, USA

*E-mail: osteinbock@fsu.edu

†Electronic Supplementary Information (ESI) available: [details of any supplementary information available should be included here]. See DOI: 10.1039/x0xx00000x

The behavior to be described here is also related to recent reports of self-propelled manganese-containing chemical garden tubes[24-26]. These structures are able to move in H_2O_2 solution through the catalytic decomposition of H_2O_2 and the ejection of small streams of oxygen bubbles.[27,28] The tubes were found to contain a sufficiently large oxygen bubble to stay buoyant, and they were consistently located just beneath the solution-air interface. In contrast, this work shows that copper-based tubes contain smaller volumes of gas and oscillate between a buoyant and a non-buoyant state. This motion primarily occurs in the vertical direction.

Buoyancy-driven vertical oscillations have also been reported for toy demonstrations (most notably the “baking powder diver”),[29,30] spherical catalytic particles, and small crystals with loosely attached surface bubbles. These reports utilized Janus-like catalyst-coated glassy carbon beads[31], pH-responsive metal-organic framework particles[32] as well as Prussian-blue-containing gel beads with the latter showing motion-correlated light emission[33]. Our study distinguishes itself from this earlier work by utilizing hollow catalyst tubes that provide a cavity for gas-mediated buoyancy regulation. In addition, we demonstrate that the tube orientations and acceleration profiles during ascent and descent are distinctive and quantifiable.

Materials and methods

Chemicals.

Copper sulfate ($CuSO_4 \cdot 5H_2O$, VWR Chemicals), sodium metasilicate ($Na_2SiO_3 \cdot 5H_2O$, Alfa Aesar), and hydrogen peroxide (H_2O_2, 30% w/v, VWR Chemicals) were used as received. All solutions were prepared with nanopure water filtered by a Barnstead Easypure UV system (resistivity: 18 MΩ cm).

Tube production.

Under ambient conditions, 0.1 M $CuSO_4$ solution was injected into 50 mL Na_2SiO_3 solution of different concentrations (0.25-1.0 M) using a syringe pump (New Era Pump Systems, NE-300). The pump rate was kept constant at 8 mL/h, and the container had a square base measuring 3.2 cm × 3.2 cm. We stopped the pump when the tip of the tube reached the floating precipitate that accumulated underneath the meniscus. Further injection lead to unwanted branched structures. The tube was then extracted, rinsed with nanopure water, and stored in a Petri dish.

Bobbing motion.

The as-prepared tube was cut with a razor blade into segments of the desired length (about 3 mm). Using a pipette, we then transferred the tube segment into a large rectangular container (8 cm×6 cm×1 cm) filled with H_2O_2 solution. The tube motion and orientation were monitored with a Nikon D3300 camera equipped with a Tamron 90mm f/2.8 macro lens. Image sequences were analyzed using in-house MATLAB scripts. All experiments were performed at room temperature.

Experimental results

We produce the precipitate tubes using the experimental setup shown in Fig. 1a, which consists of a container filled with sodium silicate solution and a glass nozzle mounted into the vessel's lower base. When copper sulfate solution is injected through the nozzle, a nearly vertical chemical garden tube forms and steadily extends upwards. This process is known as "jetting growth"[18] because the open tip of the tube ejects upward-streaming copper solution that creates additional precipitate near the air-solution interface. This precipitate can be seen as a cone-shaped structure in Fig. 1a. After a few minutes, the main tube is extracted and cut into short segments (Figs. 1b and S1). Notice that earlier studies reported the materials characterization for very similar tubes identifying $Cu(OH)_2$ as the main constituent as well as a silica-rich external surface layer that in our experiments will conveniently decrease catalytic activity on the outer tube.[21,23]

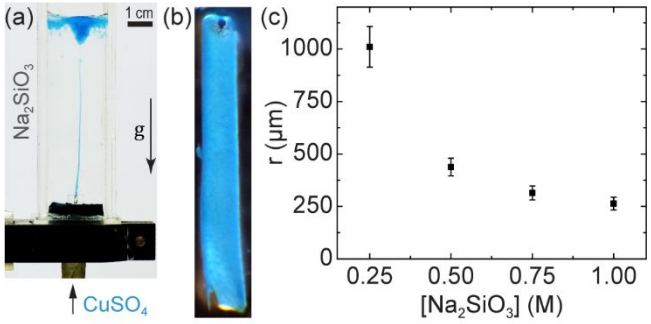

Fig. 1 (a) Experimental setup. 0.10 M $CuSO_4$ was injected into a 0.75 M Na_2SiO_3 solution. The image was captured after a 3 min injection. (b) Micrograph showing a segment of the resulted tube. Field of view: 0.6 × 3.1 cm^2. (c) Tube radius as a function of the employed silicate concentration.

We found that the tube radius can be conveniently selected by variation of the employed silicate concentration. As shown in Fig. 1c, the radius decreases from about 1 mm to 250 μm with increasing concentrations in the range of 0.25 to 1.0 M. Both the magnitude and the concentration-dependent trend agree with prior theoretical descriptions[20] of hydrodynamically controlled tube growth and is primarily caused by density and

ARTICLE

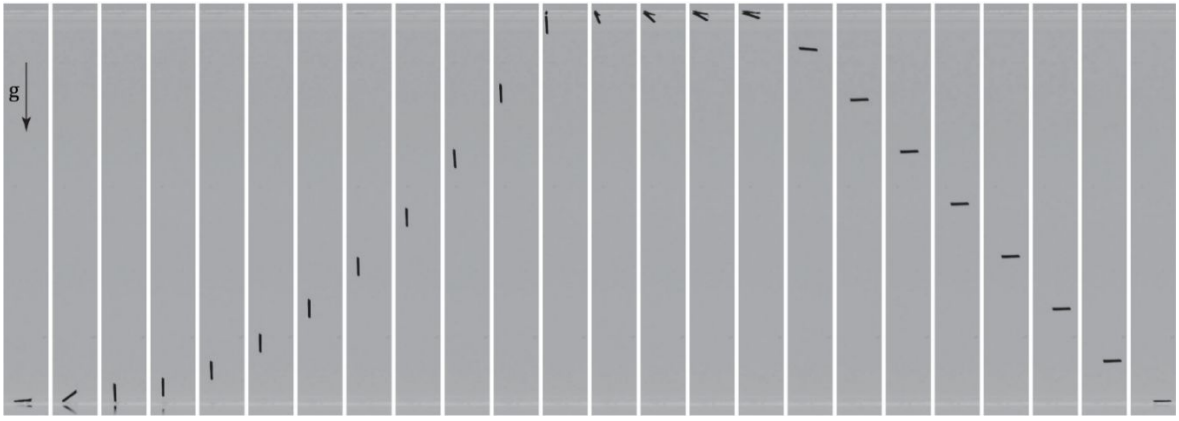

Fig. 2 Image sequence showing the bobbing motion of the tube at 0.5 s intervals. Field of view: 55 × 6 mm^2. Concentration of H_2O_2: 1 %.

viscosity changes. We also note that the tubes produced in 0.25 M silicate solution are extremely fragile, possibly due to a thinner silica layer on the outside of the tube. All of the following experiments employ tubes synthesized at 0.75 M.

When the tube segments are submerged in H_2O_2 solution, they quickly sink to the container base, remain there, and turn to olive green and eventually black within a minute. The fast but discernible color changes are indicative of blue $Cu(OH)_2$ reacting with H_2O_2 forming unstable CuO_2 that quickly reduces to stable CuO (black).[34] Notice that the synthesis of CuO from $CuCO_3 \bullet Cu(OH)_2$ in H_2O_2 solution has been previously reported.[35] As expected for CuO (and more generally Cu^{2+} ions)[36], the black tubes begin to catalyze the decomposition of the peroxide fuel into oxygen and water according to the reaction

$$2\ H_2O_2(aq) \rightarrow 2\ H_2O(l) + O_2(g). \quad (1)$$

Consequently, small amounts of oxygen gas form in the tube cavity increasing the buoyancy of the structure that without gas is heavier than the surrounding solution. More specifically, the densities[37] of crystalline CuO and amorphous SiO_2 are 6.3 g/cm^3 and 2.2 g/cm^3, respectively, and hence much greater than the density of a 30% w/w H_2O_2 solution at room temperature (1.1 g/cm^3). Notice, however, that chemical garden walls are microporous[38] and hence can be expected to have lower densities than those of the crystalline materials.

The increasing amount of oxygen gas eventually creates a net buoyant situation, and the tube lifts off from the container base rising towards the air-solution interface. During this ascent phase, the tube is nearly always in a vertical orientation as illustrated in Fig. 2 (frames 3-12). This image sequence shows side views of the container at an interval of 0.5 s. Once the tube reaches the air-solution interface, it swings into a horizontal orientation staying just underneath the interface. Accordingly, no surface pinning occurs. After several seconds of no significant motion, the tube descends again. As shown in Fig. 2 (frames 16-24), the tube assumes a horizontal orientation during this phase and subsequently lands "flat" on the container base. After another rest phase, this cycle repeats for several hours in a rhythmic fashion. Eventually, due to fuel consumption and fatigue damage to the wall material, the tube remains at the container base.

The rhythmic behavior of the tube motion is summarized in Fig. 3a (see also Movie S1). The figure consists of 51 superposed snapshots recorded during 35 s of a representative experiment. The positions and orientations are rendered in different colors that indicate the respective time according to the color bar. Notice that during the descent phases, the tube's long axis is slightly tilted with respect to a perfect horizontal orientation. We suggest that this tilt angle is associated with a horizontal displacement away from the starting position. This lateral drift is illustrated in Fig 3b where the tube's vertical coordinate z is plotted against the horizontal coordinate x. We remind the reader that the solution container is rectangular with a base measuring 6×1 cm^2 and that the x coordinate extends along this 6 cm wide dimension. Following the progression of the tube's centroid coordinate (x,z), we observe, in this example, an overall drift to the right with the largest horizontal displacement occurring during the first analyzed descent phase.

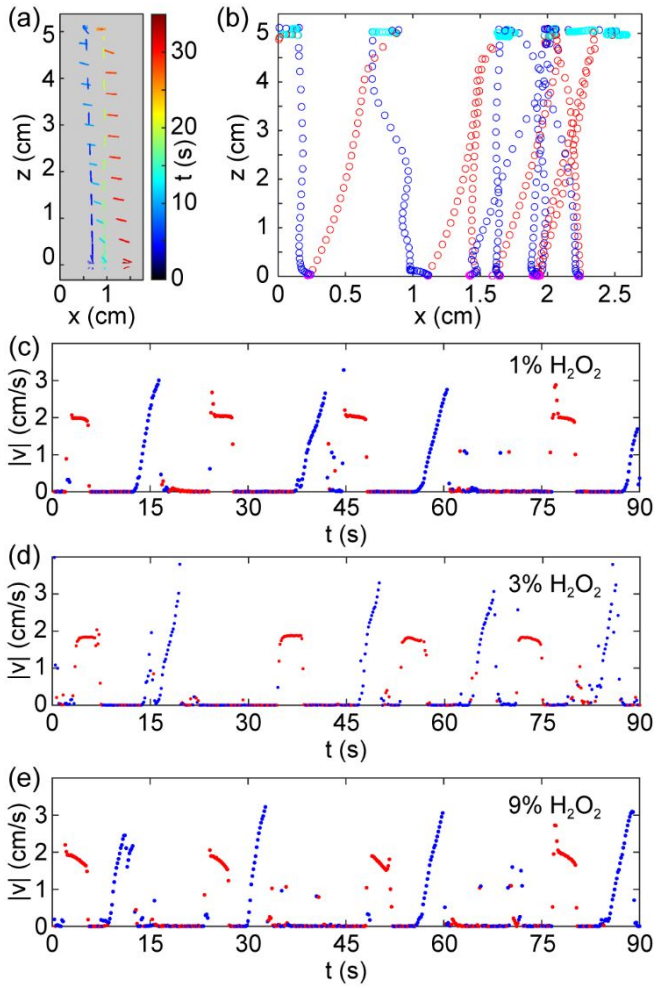

Fig. 3 (a) Time-evolution of the bobbing tube over 35 s. The tube position is color-coded according to time with blue and red indicating early and late stages, respectively. (b) Centroid coordinates of the bobbing tube over 2.5 min. Cyan, magenta, blue, and red colors indicate positions near the top, the bottom, during ascent, and during descent, respectively. A solution of 9% H_2O_2 was used in the experiment for (a,b). (c-e) Tube speed as a function of time for 1% (c), 3% (d), and 9% (e) H_2O_2. The blue and red markers correspond to upward and downward motion, respectively.

Figures 3c-e show the temporal evolution of the vertical tube speed $|v|=|dz/dt|$ for three different H_2O_2 concentrations. Blue and red markers correspond to upward and downward motion, respectively. The ascent phases are characterized by a steady acceleration that results in linearly increasing speeds. In contrast, the falling tubes show a constant velocity during the main portion of the descent. The corresponding average is about 2 cm/s. Closer inspection of these plateaus reveals a slight decrease in speed (most pronounced in (e)) with changes staying below the 10% mark of the average. Based on the available data, the average descent speed shows no dependence on the employed H_2O_2 concentration. The ascent acceleration $a=d^2z/dt^2$, however, has a mild concentration dependence. As shown in Fig. S2, the values for 1, 3, and 9% H_2O_2 are 0.75±0.07, 0.94±0.13, and 0.92±0.16 cm/s^2, respectively. Notice that the viscosities and densities of these three solutions are essentially identical.[39,40]

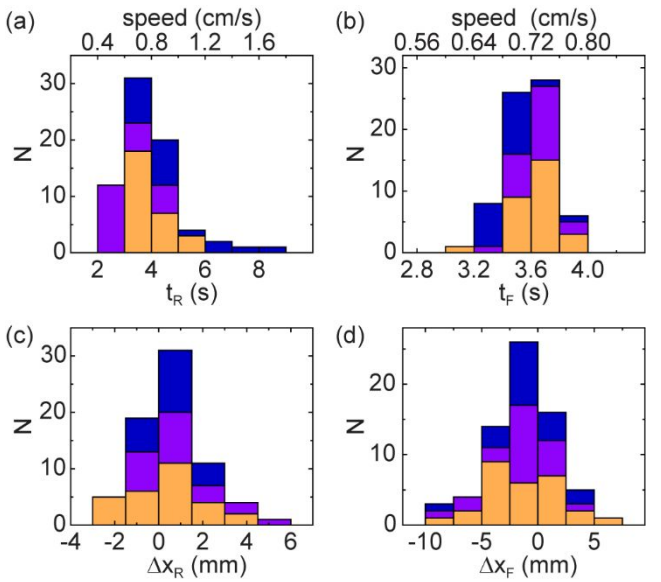

Fig. 4 Histograms of the tubes' travel time (a,b) and their horizontal displacement (c,d) per single rise (a,c) and fall (b,d). Yellow, purple, and blue bar segments correspond to H_2O_2 concentrations of 9%, 3%, and 1%, respectively.

The histograms in Fig. 4 analyze different features of the tube oscillations based on data from numerous cycles. The data obtained for three different H_2O_2 concentration are shown as blue, purple, and yellow histogram bar segments; accordingly, the total bar height does not differentiate between different conditions. Figs. 4a,b summarize the measured times of active rise (t_R) and fall (t_F), respectively. The total distribution of the rise times appears to be log-normal with a mode of 3.6 s. Notice that the data for 1% H_2O_2 (blue segments) shows the largest values which agrees with the aforementioned slower acceleration. The descent times have a smaller spread with a mean of 3.6 s and a standard deviation of 0.17 s. Considering the constant height of the solution, the data sets can also be interpreted in terms of average tube speeds (see top axes in Figs. 4a,b). These speeds are lower than the "plateau speeds" in Figs. 3c-d, because t_R and t_F are measured over the entire rise and fall phases.

Figures 4c,d summarize our measurements of the tubes' horizontal displacement during the rise and fall phases, respectively. As expected for our experiments, both data sets can be described by normal distributions with mean values near zero. We specifically find 0.58±1.52 cm for rising tubes and -1.28±3.08 cm for falling tubes. These results show that the horizontal displacement during the descent is more pronounced than during the rocket-like rise (see also Fig. 3b).

The bobbing tubes do not have a well-defined period T as their average cycle duration is determined not only by the sum of the rise and fall times, but also by the erratic rest times at the vessel base t_B and the air-solution interface t_T ($T = t_B+t_R+t_T+t_F$). The value of t_B is clearly linked to the rate of catalytic oxygen production which increases the buoyant force and eventually causes the ascent of the tube. The factors determining the value

of t_T are less clear; however, during this time, gas must be released as the tube eventually increases in effective density and commences the next descent phase.

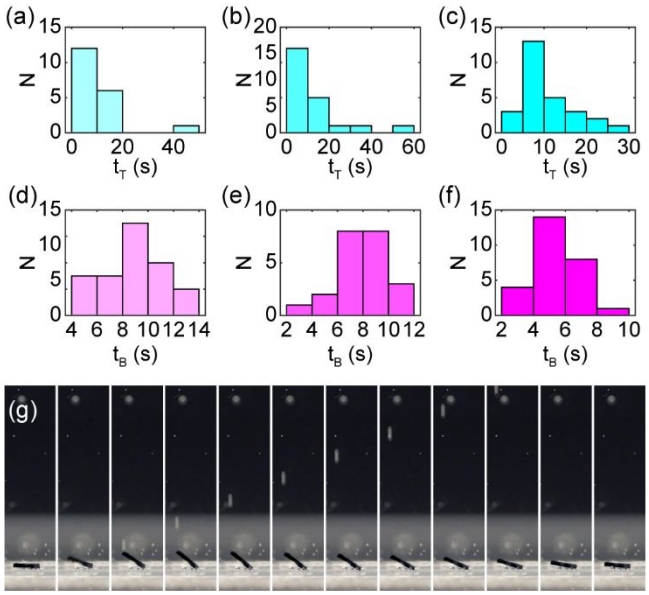

Fig. 5 Histograms of resting times at the top (a-c) and bottom (d-f) of the system. The transparency of the color bars increase with the H_2O_2 concentration: 1% (a,d), 3% (b,e), and 9% (c,f). (g) Image sequence showing the early release of a bubble and lever-like motion of a tube at the container base. This release extends the stay at the bottom. Concentration of H_2O_2: 1%. Field of view: 5 mm × 20 mm. Time interval between frames: 33 ms.

Figures 5a-f are histograms summarizing our measurements of t_T (a-c) and t_B (d-f) for H_2O_2 concentrations of 1% (a,d), 3% (b,e), and 9% (c, f). The average values are t_T = 9.8, 12.1, 11.0 s for (a-c) and t_B = 9.0, 8.0, 5.4 s for (d-f), respectively and show longer rest times at the air-solution interface than on the container base ($t_T > t_B$). Notice that the t_B values decrease with increasing H_2O_2 concentration which agrees with the expected faster gas production at higher concentration. In addition, t_T varies more strongly than t_B.

One of the factors affecting t_B is illustrated in the image sequence of Fig. 5g. During t_B, the gas-producing tubes undergo a tilting motion that lifts one of its orifices off the base; however, this tilt can release the gas from the tube producing a small upward rising bubble (poorly resolved but clearly discernible in frames 3-10). In response, the—now heavier tube—sinks back to the base and re-establishes its horizontal position. Accordingly, successful lift-off and ascent require that the oxygen bubble remains within in the tube cavity. This requirement must be related to a suitable pinning site either within the cavity or near the edge of the orifice. Lastly, we note that this pinning of the interior bubble can occasionally fail during the rise phase, which aborts the ascent and causes the tube to return to the container base (Fig. S3).

Theoretical results

Our experiments revealed well defined patterns for the movement of ascending and descending tubes. We will now discuss this vertical motion in terms of the tube wall's weight F_w within the solution, the buoyant force F_b caused by the oxygen gas in the tube cavity, and the drag force F_d. Our model equations assume Stokes or creeping flow (Reynolds number Re < 1) for which inertial forces are small compared to viscous forces. This condition is marginally met for ascending tubes (Re ≈ 6) but descending tubes (Re ≈ 60) likely create a small vortex pair in their wake, which increase the drag coefficient above the analyzed values.[41,42] This non-turbulent transitional behaviour is difficult to capture theoretically. As it also does not promise to provide meaningful insights, it was not considered.

We assume a wall thickness of w = 8 µm and a tube radius of r = 300 µm. The density of the tube wall and the solution are set to ρ_t = 4500 kg/m^3 and ρ_s = 1000 kg/m^3, respectively. The tube length is L = 3 mm and g = 9.8 m/s^2 denotes the acceleration due to Earth's gravity. Furthermore, we express the amount of oxygen gas within the tube cavity by the dimensionless factor $\phi \in [0,1]$ for which ϕ = 0 indicates no gas and ϕ = 1 implies that the entire cavity is filled with gas. Considering that $w \ll r$, we find

$$F_w = 2\pi r w L(\rho_t - \rho_s)g \quad , \tag{2}$$

$$F_b = \pi r^2 L \phi \rho_s g \quad . \tag{3}$$

The drag force depends on the vertical speed v and the orientation of the tube. We denote this force as $F_d^{||}$ for the rocket-like ascent and $F_d^{\perp}$ for the flat descent. Using prior analyses of solid rods given in refs. [43-46], these forces are described by

$$F_d^{||} = -\frac{2\pi\mu L}{ln\frac{L}{2r} + \gamma_{||}} v \quad , \tag{4}$$

$$F_d^{\perp} = -\frac{4\pi\mu L}{ln\frac{L}{2r} + \gamma_{\perp}} v \quad , \tag{5}$$

with dimensionless constants $\gamma_{||}$ = –0.114, $\gamma_{||}$ = 0.886, and the solution viscosity μ = 1×10^{-3} Pa s. The mass m and the acceleration dv/dt of the system (assumed to be the tube and its interior solution volume) are given by

$$m = 2\pi r w L \rho_t + \pi r^2 L(1-\phi)\rho_s \quad , \tag{6}$$

$$m\,\mathrm{dv/dt} = F_b - F_w + F_d \quad . \tag{7}$$

For constant ϕ, we can calculate the terminal velocity of the tube and find that this speed is reached very rapidly (< 0.2 s). Accordingly, the bobbing motion is controlled by the tube buoyancy which, for ascending tubes, must increase steadily to yield a constant acceleration. The falling tubes, however, maintain a nearly constant F_b and move at the corresponding constant terminal speed. We explain this difference by fresh reactant solution gently replacing the H_2O_2-depleted liquid in the case of vertically aligned, rising tubes (see Discussion for details). This injection of new fuel effectively increases the gas volume and enhances the buoyancy via an increase in ϕ.

As the expected change in ϕ is small during the short ascent time, we describe the O_2 production as a zeroth order process with a rate constant k:

$$\frac{d\phi}{dt} = k \quad . \qquad (8)$$

We re-emphasize that for horizontally oriented, falling tubes, this kinetic factor is essentially absent (i.e. $k \approx 0$). For situations with large variations in ϕ (e.g. rising tubes in deeper solutions), a rate of $k'(1-\phi)$ could be considered to describe the decrease in the solution-exposed catalytic surface during gas production; however, a distribution of the gas volume to multiple small bubbles would diminish the effect of a ϕ-dependent reduction in catalytic area.

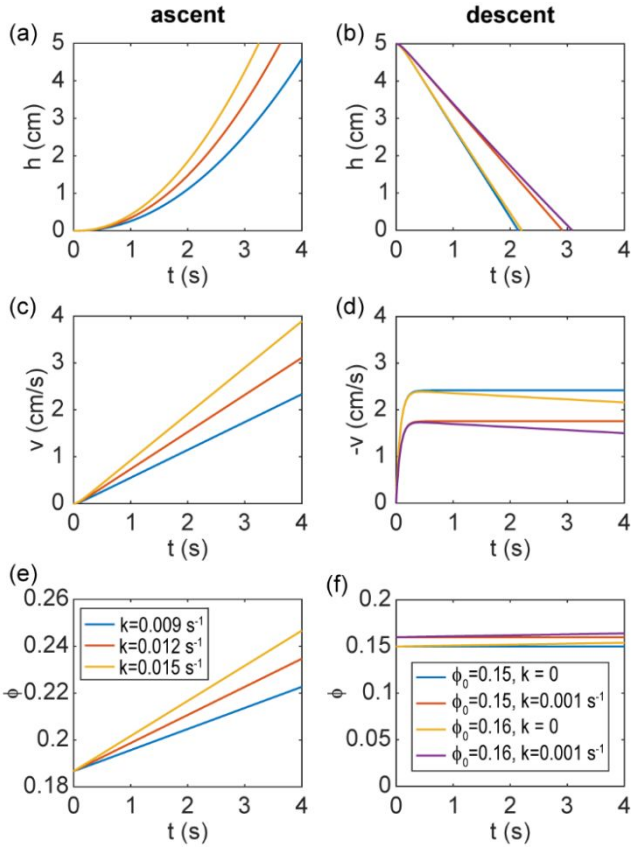

Fig. 6 Calculated time-dependence of the vertical position h (a,b), velocity v (c,d), and gas volume fraction ϕ (e,f) for ascending (a,c,d) and descending tubes (b,e,f). The calculations consider weight, buoyancy, and drag force while only assuming a rate constant k for the catalytic gas production and, for descending tubes, an initial ϕ value (see legends). The calculated motion captures the experimental results (Fig. 3) quantitatively.

Figure 6 shows the evolution of the tube height h, speed $|v|$, and gas fraction ϕ for rising (a,c,e) and falling tubes (b,d,f) as calculated on the basis of eqs. 2-8. The graphs in the left column are calculated for initially resting and weightless ($F_w = F_b$) tubes. They show the dynamics for three different rate constants (k = 0.009, 0.012, and 0.015 s^{-1}). After a short transient phase of about 0.2 s (Fig. S4), the time-dependent height $h(t)$ traces parabolas and reaches h = 5 cm (the layer height in our experiments) within 3-4 s. Accordingly, the tube velocity increases linearly and the final values for h = 5 cm are near the experimental maximum of 3 cm/s. During the ascent, the gas volume fraction increases by about 20%. Clearly, the calculations do not account for orientational changes of the tube during lift-off and arrival at the air-solution interface.

Our calculations for descending tubes (right column of Fig. 6) assume initial ϕ values of 0.15 and 0.16 that are either constant (k = 0) or increase very slowly with k = 0.001 s^{-1}. The latter rate constant is about ten times smaller than the k values considered for the tube ascent. These values reproduce the experimentally observed steady descent at a constant speed of about 2 cm/s (compare to Fig. 3). As mentioned earlier, this terminal velocity is reached rapidly (< 0.2 s, Fig. 6d). In addition, the traces for k = 0.001 s^{-1} show that the minor decrease in the descent speed (occasional downward slopes of blue plateaus in Fig. 3) is caused by a very slow gas production during the descent. While not studied further, this secondary effect might relate to the tilt angle of the falling tube, which provides different degrees of weak fuel injection.

Discussion

Our study of the rhythmic bobbing motion of chemical garden tubes raises several questions that require further discussion. A perplexing point of our analysis is related to the concentration dependence of the rate constant k. Our measurements show that the acceleration of the ascending tube is essentially independent of the employed H_2O_2 concentration (Fig. S2). This finding suggests that the catalytic gas production in the cavity is controlled by the available surface area and that even at the lowest investigated concentration of 1%, the H_2O_2 level is sufficiently high to not affect the reaction rate significantly. However, our model assumes that the constant acceleration of ascending tubes arises from the injection of fresh fuel whereas descending tubes move at constant speeds due to a lack of fresh H_2O_2. This assumption clearly implies a concentration dependence of the reaction rate as it distinguishes between fresh and (partially) depleted fuel levels.

We propose the following interpretation to resolve this seeming contradiction. We suggest that the gas volume in the tube cavity is distributed over several small bubbles rather than a large plug-like gas volume. This presence of small bubbles allows for an actual throughflow of fresh solution during the ascent phase (diffusive transport is irrelevant considering the tube length of 3 mm and average rise time of 4 s). Accordingly, the H_2O_2 concentration within the cavity is only slightly diminished with respect to the surrounding solution and remains bound to the kinetic zeroth-order limit. For descending tubes, however, this throughflow does not occur because the tubes are in a nearly horizontal orientation. Accordingly, the descending tubes must have depleted their fuel levels to the point that k has become concentration dependent and the resulting gas production is negligible.

While this interpretation clarifies the changes of the effective rate constant *k* between ascent and descent phases, it also reveals a, somewhat hidden, simplification in our analysis. If correct, the slow solution flow through the ascending tube complicates our original assumption that the forces act on a mass system formed by the tube wall and its interior solution (see eq. (6)) as this flowing solution is not fully tied to the tube wall. More detailed analyses of the involved fluid dynamics are needed to unravel this difficulty.

Another question concerns the inability of silica-CuO tubes to perform sustained horizontal self-propulsion even at a relatively high H_2O_2 concentration of 9%. This differs profoundly from the motion of similarly sized silica-MnO_2 chemical garden tubes which remain buoyant and self-propel underneath the air-solution interface for H_2O_2 concentrations as low as 1%.[24] It is tempting to interpret this finding in terms of a lower catalytic activity of CuO and consequently a lower production rate of oxygen gas; however, a lower rate would simply increase the time to reach buoyancy and not prevent the tube from reaching the air-solution interface, where it could, in principle, self-propel horizontally at a lower rate of bubble ejection and hence a lower average speed. Therefore, we suggest that the difference between the two motion types relates to the tubes' surface textures. The surface of Mn-based tubes is known to be rough and flaky[24] providing a large number of pinning sites and crevices for bubbles to attach to; the Cu-based tubes appear much smoother and hence disfavor bubble pinning. This surface-specific difference results on average in a lower buoyancy of the silica-CuO tubes and is hence at the heart of the observed bobbing motion.

A third, and possibly related, question concerns the long times t_T that silica-CuO tubes spend underneath the air-solution interface prior to descent. Our results indicate durations of up to 1 min, whereas sunken tubes can release several bubbles during much shorter t_B intervals. As there is no reason to assume that risen tubes should cease oxygen production, the question of a capsizing mechanism must fall again to the release of a sufficiently large fraction of the tube-bound gas volume and, therefore, to the specific pinning of the oxygen bubbles to the interior wall surface. Unlike tubes at the base that can perform a lever-like motion, risen tubes maintain a horizontal orientation and, therefore, gas is only expelled due to an excessive gas volume or a random movement of the tube. Closer inspection of the data in Fig. 3b reveals this motion in the stretched-out segments of the cyan markers that largely exceed the horizontal displacement of sunken tubes (magenta markers). The detailed processes giving rise to a sufficiently large drop in buoyancy remain unclear.

A fourth question pertains to the horizontal displacement of falling tubes (Δx_F), which can reach 1 cm and on average exceeds the horizontal displacement during the ascent phase (Δx_R). Considering the standard deviations of the measured distributions (Figs. 4c,d), we find that the horizontal displacement is on average 2.2 times larger during the descent phase. This difference is most likely linked to the different orientations of the rising and falling tubes. We note that the latter motion has been studied for ellipsoids and solid rods such as sinking cylindrical plankton and pencil lead.[47] In this context, a small tilt of the sinking tube away from a perfect horizontal orientation (Fig. 2) is of importance as it increases the expected displacement. It seems likely that this tilt is not only caused by fluid dynamics, but also by the detailed distribution of the small residual gas volume within the tube. We emphasize that our interpretation of the gas volume as multiple small bubbles is the most convincing explanation for the constant weight distribution along the horizontal tube, as other explanations would require either a centered single bubble or no gas at all.

Lastly, we discuss the tube position with regard to the 1-cm depth *y* of the container that was not resolved in our experiments. Surprisingly, the perceived tube length in our images matched the actual length and we only rarely captured descending tubes pointing away from the camera. These qualitative observations indicate a preferential alignment of both the buoyancy-losing and sinking tube along the *x*-direction. This alignment is clearly caused by the solution meniscus and as the tube's buoyancy is at a marginal level prior to the start of the descent phase, it suggests a centering of the tube to positions with $y \approx 0.5$ cm. Accordingly, disturbances of the descent motion by wall effects[48] are intrinsically minimized by the experimental system.

Conclusions

Our study brought together three previously unrelated research areas by showing that chemical garden structures can exhibit chemical oscillations that enable chemical self-propulsion. We found that the vertical motion of these structures is accurately explained by reaction-induced changes of their internal oxygen volume. The resulting buoyancy-driven motion is akin to the depth control of fish or submarines and differs clearly from earlier propulsion mechanisms of catalytic tubes[24-28] which relied on the ejection of gas bubbles. The behavior of the structures during their resting periods was stochastic and will require further investigation. This future research could be extended to work on collective phenomena in systems with large numbers of bobbing tubes, as well as potential applications of these structures for mixing and catalytic processing.

Author contributions

Qingpu Wang: conceptualization, methodology, formal analysis, investigation, data analysis, visualization, writing – review & editing. Oliver Steinbock: conceptualization, funding acquisition, supervision, methodology, formal analysis, writing – review & editing.

Conflicts of interest

There are no conflicts to declare.

Acknowledgements

The material is based upon work supported by the National Science Foundation under grant No. 1565734 and NASA under grant No. 80NSSC18K1361.

Notes and references

1 I. R. Epstein and J. A. Pojman, *An Introduction to Nonlinear Chemical Dynamics: Oscillations, Waves, Patterns, and Chaos*, Oxford University Press, 1998.
2 M. T. Fechner, *Schweiggers Journal für Chemie und Physik*, 1828, **53**, 129-151.
3 G. Nicolis and J. Portnow, *Chem. Rev.*, 1973, **73**, 365-384.
4 G. Nicolis and I. Prigogine, *Exploring Complexity: An Introduction,* W.H. Freeman, 1989.
5 I. R. Epstein, K. Kustin, P. De Kepper and M. Orbán, *Sci. Am.*, 1983, **248**, 112-123.
6 A. T. Winfree, *The Geometry of Biological Time*, Springer, 1980.
7 K. Krischer and H. Varela, *Handbook of Fuel Cells*, Wiley, 2010.
8 G. Ertl, *Angew. Chem. Int. Ed.*, 2008, **47**, 3524-3535.
9 B. A. Grzybowski, *Chemistry in Motion. Reaction-Diffusion Systems for Micro- and Nanotechnology,* Wiley, 2009.
10 O. Steinbock, A. Lange and I. Rehberg, *Phys. Rev. Lett.*, 1998, **81**, 798.
11 V. V. Yashin and A. C. Balazs, *Science*, 2006, **314**, 798-801.
12 J. Horváth, I. Szalai, J. Boissonade and P. De Kepper, *Soft Matter*, 2011, **7**, 8462-8472.
13 L. M. Barge, S. S. Cardoso, J. H. Cartwright, G. J. Cooper, L. Cronin, A. De Wit, I. J. Doloboff, B. Escribano, R. E. Goldstein and F. Haudin, *Chem. Rev.*, 2015, **115**, 8652-8703.
14 J. Pantaleone, A. Toth, D. Horvath, L. RoseFigura, W. Morgan and J. Maselko, *Phys. Rev. E*, 2009, **79**, 056221.
15 C. Collins, R. Mokaya and J. Klinowski, *Physical Chemistry Chemical Physics*, 1999, **1**, 4669-4672.
16 J. H. E. Cartwright, J. M. García-Ruiz, M. L. Novella and F. Otálora, *J. Colloid Interface Sci.*, 2002, **256**, 351-359.
17 B. C. Batista, P. Cruz and O. Steinbock, *Langmuir*, 2014, **30**, 9123-9129.
18 S. Thouvenel-Romans and O. Steinbock, *J. Am. Chem. Soc.*, 2003, **125**, 4338-4341.
19 E. Nakouzi and O. Steinbock, *Sci. Adv.*, 2016, **2**, e1601144.
20 S. Thouvenel-Romans, W. v. Saarloos and O. Steinbock, *Europhys. Lett.*, 2004, **67**, 42.
21 J. J. Pagano, S. Thouvenel-Romans and O. Steinbock, *Phys. Chem. Chem. Phys.*, 2007, **9**, 110-116.
22 B. C. Batista and O. Steinbock, *Chem. Commun.*, 2022, **58**, 12736-12739.
23 L. Roszol, R. Makki and O. Steinbock, *Chem. Commun.*, 2013, **49**, 5736-5738.
24 Q. Wang, P. Knoll and O. Steinbock, *J. Phys. Chem. B*, 2021, **125**, 13908-13915.
25 P. Kumar, Q. Wang, D. Horváth, Á. Tóth and O. Steinbock, *Soft Matter*, 2022, **18**, 4389-4395.
26 Q. Wang and O. Steinbock, *Phys. Chem. Chem. Phys.*, 2022, **24**, 14538-14544.
27 A. A. Solovev, Y. Mei, E. Bermúdez Ureña, G. Huang and O. G. Schmidt, *Small*, 2009, **5**, 1688-1692.
28 J. Li, I. Rozen and J. Wang, *ACS Nano*, 2016, **10**, 5619-5634.
29 B. J. Derr, H. R. Derr, T. Lewis and H. Tom, *J. Chem. Educ.*, 2000, **77**, 171.
30 B. Rohrig, *Sci. Teach.*, 2001, **68**, 38-41.
31 M. Wu, Y. Koizumi, H. Nishiyama, I. Tomita and S. Inagi, *RSC Adv.*, 2018, **8**, 33331-33337.
32 Z. Guo, T. Wang, A. Rawal, J. Hou, Z. Cao, H. Zhang, J. Xu, Z. Gu, V. Chen and K. Liang, *Mater. Today*, 2019, **28**, 10-16.
33 R. María-Hormigos, A. Escarpa, B. Goudeau, V. Ravaine, A. Perro and A. Kuhn, *Adv. Mater. Interfaces*, 2020, **7**, 1902094.
34 I. I. Volnov, *Peroxides, Superoxides, and Ozonides of Alkali and Alkaline Earth Metals*, Springer, 1966.
35 T. X. Wang, S. H. Xu and F. X. Yang, *Powder Technol.*, 2012, **228**, 128-130.
36 J. F. Perez-Benito, *Monatsh. Chem.*, 2001, **132**, 1477-1492.
37 L. B. Railsback, *Some Fundamentals of Mineralogy and Geochemistry, http://railsback.org/FundamentalsIndex.html*, (accessed September 2021).
38 D. Balköse, F. Özkan, U. Köktürk, S. Ulutan, S. Ülkü and G. Nişli, *J. Sol-Gel Sci. Technol.*, 2002, **23**, 253-263.
39 M. F. Easton, A. G. Mitchell and W. F. K. Wynne-Jones, *Trans. Faraday Soc.*, 1952, **48**, 796-801.
40 G. Goor, J. Glenneberg, S. Jacobi, J. Dadabhoy and E. Candido, in *Ullmann's Encyclopedia of Industrial Chemistry*, Wiley, 2019, pp. 1-40.
41 G. Bagheri and C. Bonadonna, *Powder Technol.*, 2016, **301**, 526-544.
42 C. E. Brennen, *An Internet Book on Fluid Dynamics - Drag on a Sphere and Cylinder*, http://brennen.caltech.edu/fluidbook/externalflows/drag/dragonasphere.pdf, (accessed February 2023).
43 K. Yang, C. Lu, X. Zhao and R. Kawamura, *PLoS One*, 2017, **12**, e0188015.
44 R. Cox, *J. Fluid Mech.*, 1970, **44**, 791-810.
45 A. T. Chwang and T. Y.-T. Wu, *J. Fluid Mech.*, 1975, **67**, 787-815.
46 J. Tillett, *J. Fluid Mech.*, 1970, **44**, 401-417.
47 D. P. Holland, *J. Plankton Res.*, 2010, **32**, 1327-1336.
48 H. Brenner, *J. Fluid Mech.*, 1962, **12**, 35-48.

